Lipocalin-2-mediated Astrocyte Pyroptosis promotes neuroinflammatory injury via NLRP3 Inflammasome Activation in Cerebral Ischemia/Reperfusion Injury

Juanji Li
Medical School of Nanjing University
Pengfei Xu
The First Affiliated Hospital of USTC, University of Science and Technology of China
Ye Hong
Nanjing Medical University
Yi Xie
Medical School of Nanjing University
Mengna Peng
Medical School of Nanjing University
Rui Sun
Shanghai Changhai Hospital, Second Military Medical University, Naval Medical University
Hongquan Guo
Southern Medical University
Xiaohao Zhang
Nanjing Medical University
Wusheng Zhu
Medical School of Nanjing University
Junjun Wang
Medical School of Nanjing University
Xinfeng Liu (xfliu2@vip.163.com)
Medical School of Nanjing University

Research Article

Keywords: cerebral ischemia/reperfusion injury, astrocyte, pyroptosis, LCN2, NLRP3 inflammasome

Posted Date: February 24th, 2023

DOI: https://doi.org/10.21203/rs.3.rs-2606918/v1

Additional Declarations: No competing interests reported.

Version of Record: A version of this preprint was published at Journal of Neuroinflammation on June 23rd, 2023. See the published version at https://doi.org/10.1186/s12974-023-02819-5.

Abstract

Background: Neuroinflammation has been recognized as vital pathophysiological process during ischemic stroke. Activated astrocytes play a major role in inflammatory response. Lipocalin-2 (LCN2), secreted from activated astrocytes, promotes neuroinflammation. Pyroptosis, a pro-inflammatory programmed cell death, is emerging as a new area of research on stroke. Nevertheless, the potential role of LCN2 in astrocyte pyroptosis remains unclear.

Methods: Ischemic stroke model was established by middle cerebral artery occlusion (MCAO) *in vivo*. *In vitro*, oxygen-glucose deprivation and reoxygenation (O/R) was applied to cultured astrocytes. 24p3R (the LCN2 receptor) was inhibited by astrocyte-specific adeno-associated virus (AAV-GFAP-24p3Ri). We used MCC950 and Nigericin sodium salt (Nig) to inhibit or promote the activation of NLRP3 inflammasome pharmacologically. Histologic and biochemical analysis was performed on the death of astrocytes and neurons both *in vivo* and *in vitro*. Besides, the neurological deficit of mice was evaluated.

Results: LCN2 expression was significantly induced in astrocytes 24 hours after stroke onset in mouse MCAO models. *Lcn2* knockout ($Lcn2^{-/-}$) mice exhibited reduced infract volume and improved neurological and cognitive functions after MCAO. LCN2 and its receptor 24p3R were colocalized in astrocytes. Mechanistically, suppression of 24p3R by AAV-GFAP-24p3Ri alleviated pyroptosis pores formation and pro-inflammatory cytokines secretion induced by LCN2, which was then reversed by NLRP3 inflammasome activation inducer Nig. Astrocyte pyroptosis was exacerbated in $Lcn2^{-/-}$ mice by intracerebroventricularly administration of recombinant LCN2 (rLCN2), while the aggravation was restricted by blocking 24p3R or inhibiting NLRP3 inflammasome activation by MCC950.

Conclusion: LCN2/24p3R mediates astrocyte pyroptosis via NLRP3 inflammasome activation following cerebral ischemia/reperfusion injury.

Introduction

Cerebral ischemia/reperfusion injury can trigger grievous inflammatory response [1]. Astrocytes emerge as key players in neuroinflammatory procedure [2]. Previous studies have shown that astrocytes play a central role in inflammatory pathology by communicating with CNS-resident cells, such as microglia [3–5], or CNS-infiltrating cells [6, 7]. In recent years, a new pro-inflammatory programmed cell death called pyroptosis is appealing. Pyroptosis, a caspase-1 mediated programmed cell death, is characterized by GSDMD membrane pores formation, cell swelling and efflux of cytoplasmic pro-inflammatory cytokines [8, 9]. Inflammasome activation, such as NLRP3, is necessary for pyroptosis [8]. To date, several studies have found that astrocyte pyroptosis was induced by cerebral ischemia insult and suppression of pyroptosis exhibited anti-inflammatory and neuroprotective function [10–13]. However, the upstream regulator of astrocyte pyroptosis has not been thoroughly reported.

Lipocalin-2 (LCN2), a member of the lipocalin family [14], functions as the acute-phase protein following brain injury [15, 16]. In the CNS, astrocytes are the primary source and target of LCN2 under brain injury

conditions [17, 18]. Our previous study has shown that LCN2 can induce astrocyte activation and exacerbate inflammatory injury in cerebral ischemia [19], which may function through facilitating pro-inflammatory cytokines production [20, 21]. LCN2 has also been reported to modulate cell death, such as apoptosis [17, 22] and autophagy [23]. The potential role of LCN2 in astrocyte pyroptosis remains to be further explored. Thus, this research aimed to investigate whether LCN2 was involved in pyroptosis of astrocytes and whether this involvement was associated with NLRP3 inflammasome activation after cerebral ischemia/reperfusion injury.

Materials And Methods

Animal

Male C57BL/6J mice weighted 20-25 g were used for the experiments *in vivo*. Wild type mice were purchased from Model Animal Research Institute of Nanjing University (Nanjing, China), and *Lcn2* knockout (*Lcn2*$^{-/-}$) mice (B6.129P2-Lcn2tm1Aade/AkiJ, Jax) were provided by the Jackson Laboratory. All mice were housed under appropriate condition (temperature 23 ± 2°C, humidity 55-60%, with 12 h-light-dark circle) with free access to food and water.

Animal model of cerebral ischemia/reperfusion injury

Transient middle cerebral artery occlusion (MCAO) were performed following previous methods [24]. In brief, the mice were anaesthetized with 2% isoflurane in O_2. Then we separated right common carotid artery (CCA), right external carotid artery (ECA) and right internal carotid artery (ICA) carefully through a middle anterior neck incision. CCA and ECA were ligated with 6-0 suture. Next, we inserted silicone coated nylon thread (diameter: 0.16 ± 0.02 mm) from a small cut on ECA into ICA to block the bifurcation of middle cerebral artery (MCA). After blocking blood flow for 90 minutes, nylon thread was extracted for reperfusion. A heating pad was used to maintain body temperature during the whole procedure. For the sham-operated mice, the same procedures were applied except the occlusion of MCA.

Brain infract volume determination

The infract volume was confirmed by 2, 3, 5-triphenyltetrazoliumchloride (TTC, Sigma, USA) staining 24 h after MCAO. Brain was cut into 1 mm-thick slices and then stained with 2% TTC solution at 37°C for 15 min at dark, followed by being fixed with 4% paraformaldehyde (PFA) at 4°C overnight [25]. We used HP Scanjet G3110 to scan the brain slices, the relative infract volume was calculated by ImageJ software (1.50g, Wayne Rasband, National Institutes of Health, USA). As reported before, the relative infract volume was calculated as: (contralateral hemisphere volume - normal ipsilateral hemisphere volume) / (contralateral hemisphere volume * 2) * 100% [25].

Neurological deficit evaluation and behavioral analysis

The modified Neurologic Severity Score (mNSS) was applied to evaluate neurological deficit after MCAO [26]. mNSS assessment system consists with four kinds of tests: motor tests, sensory tests, beam balance tests, and reflexes absent and abnormal movements. mNSS score ranges from 0 to 18. Score 0 means no neurological deficit and score 18 represents the most severe deficit.

Morris Water Maze (MWM) test was performed to evaluate spatial learning and memory ability [27]. A blind test was conducted to exclude blind mice and severely dyskinetic mice at the day 22 after MCAO. Four group mice (n = 10 per group) were trained to find the platform in four trails for consecutive 5 days from day 23 to day 27. The trail ended if the mice found the platform within 60 s. The mice would be guided to the platform and remained there for 10 s to strengthen memory if failed to find the platform. The escape latency to find the platform and the swimming pathlength were recorded. At the day 28, the platform was removed for probe trail, each trail lasted for 60 s. The time spent in the target quadrant and platform crossovers were tracked and analyzed by the ANY-maze video tracking software (Stoelting, USA).

Adeno-associated virus injection and drug administration

Astrocyte-specific Adeno-associated virus (AAV) was constructed by Shanghai Genechem Co.,Ltd. (Shanghai, China). AAV construction was used to interfere 24p3R expression. The following sequences were used: AAV-GFAP-24p3Ri 5-TCTGTATCCTCAGCATCAT-3; and AAV-GFAP-GFP 5-AGA-TTCTCCGAACGTGTCACGT-3. The AAV-GFAP-24p3Ri titers were 1.09 E+13 (copies/ml) and AAV-GFAP-GFP with 1.56 E+13 (copies/ml) of titers. AAV-GFAP-24p3Ri or AAV-GFAP-GFP was injected into right lateral ventricle (dose: 5ul, coordinates: a/p, + 0.8, m/l, + 1.2, d/v, - 2.0) 4 weeks before MCAO surgery. We injected 10 μl of 1 μg/ml recombinant LCN2 (rLCN2) (Abcam, UK) into right lateral ventricle for continuous 5 days before MCAO surgery [28]. Nigericin sodium salt (Nig) (Selleck, USA) and MCC950 (Selleck, USA) are the inducer and inhibitor of NLRP3 inflammasome activation respectively. The mice were treated with Nig (4 mg/kg, i.p) [29] or MCC950 (50 mg/kg, i.p) [30] immediately following MCAO surgery.

Primary astrocytes culture

Primary cortical astrocytes were cultured and purified on the basis of methods described previously [31]. In short, astrocytes were harvested from neonatal mice within 24 h after birth. We isolated bilateral cerebral cortex in Hank's balanced salt solution (HBSS, Gibco, USA) on ice and then stripped meninges and blood vessels under a microscope. The tissue was digested with 0.125% trypsin-EDTA (Gibco, USA) for 15 min in 37°C. The digestion was terminated with Dulbecco's Modified Eagle Medium (DMEM, high glucose, Gibco, USA) containing 10% fetal bovine serum (FBS, Gibco, USA). The mixture was pipetted for 100 times to homogenize and then filtered with screen cloth (diameter, 100 μm). After centrifuging at 1000 RPM for 5 min, the cells were resuspended with complete medium (DMEM containing 10% FBS and 1% penicillin-streptomycin) and seeded in T75 cell culture flask (corning, USA) which was previously coated with Poly-D-Lysine (PDL, sigma, USA) overnight. Twenty-four hours later, the medium was changed to clear away non-adherent cells. From hereafter, half of the medium was changed every 3 days

until cell fused totally. In order to harvest purified astrocytes, the cells were shacked in 37°C at 400 RPM for 6 h. The floating cells were washed by sterile phosphate buffer saline (PBS) for three times. The adherent cells were digested with 0.25% trypsin-EDTA for 3 min in room temperature and the digestion was stopped with complete medium. Resuspended cells were seeded in dish and medium changing was performed every 3 days.

Oxygen-glucose deprivation/reoxygenation

For oxygen-glucose deprivation (OGD), the medium was replaced with glucose-free and FBS-free DMEM (Gibco, USA). The cells were incubated in anaerobic chamber equipped with AnaeroPack-Anaero (MGC, Japan) at 37°C in constant temperature incubator. According to the time point reported previously [19], astrocytes were returned to normal culture condition for reoxygenation after 6 hours (OGD/R).

Western blotting

Total protein was extracted from penumbra region and cultured astrocytes using RIPA lysis buffer (Cell Signaling Technology, USA) for following western blotting (WB) as reported previously [32]. The protein concentration was detected by BCA kit (Generay Biotechnology, China). The protein sample was loaded into 8-12% sodium dodecyl sulfate-polyacrylamide gel electrophoresis (SDS-PAGE) for electrophoresis, and then transferred to polyvinylidene difluoride (PVDF) membranes (Millipore, USA). The membranes were incubated at 4°C overnight with primary antibodies against GFAP (1:5000, Abcam, UK), LCN2 (1:200, Abcam, UK), 24p3R (1:500, Biorbyt, UK), NLRP3 (1:500, Abcam, UK), ASC (1:500, Santa Cruz Biotechnology, USA), caspase-1(1:500, Abcam, UK), GSDMD (1:500, Santa Cruz Biotechnology, USA), IL-1β (1:500, Santa Cruz Biotechnology, USA), IL-18 (1:500, Abcam, UK), β-actin (1:5000, Cell Signaling Technology, USA). Next day, the membranes were incubated with corresponding HRP-conjugated secondary antibody at room temperature for 1 h. The optical signal was detected by enhanced chemiluminescence (Millipore, USA) and the results were analyzed by ImageJ software. β-actin was selected to serve as housekeeping gene.

Immunofluorescence staining and TUNEL staining

The mice were sacrificed after perfusion and brains were fixed with PFA at 4°C overnight. The dehydration procedure was proceeded according to the concentration gradient (10%, 20%, and 30% of sucrose solutions) at 4°C. After frozen in optimal cutting temperature compound (Sakura Finetek, Japan), the brains were sliced into 10 μm sections for immunofluorescence staining (IF).

Brain slices and cell climbing sheets were washed by PBS for three times before fixation with PFA for 10 min at room temperature. The slices were blocked with solution containing 0.1% Triton-100 (Sigma, USA), 10% goat serum (Beyotime, China) and 1% bovine serum albumin (BSA, AMRESCO, USA) for 1 h. The slices were incubated with primary antibody against GFAP (1:1000, Abcam, UK), NeuN (1:500, Abcam, UK), LCN2 (1:200, Abcam, UK), 24p3R (1:100, Biorbyt, UK), NLRP3 (1:200, Abcam, UK), ASC (1:200, Santa Cruz Biotechnology, USA), caspase-1(1:500, Abcam, UK), GSDMD (1:200, Santa Cruz Biotechnology, USA)

at 4°C overnight, followed by incubation with appropriate Alexa Fluor-488/594/647-conjugated secondary antibodies (Jackson ImmunoResearch, USA) for 1 h protected against exposure to light. After triple washing with PBS, slices were mounted with CC/MOUNT (Sigma, USA). Images were shot by a fluorescence microscope (Olympus MX51, Japan) or FluoView FV3000 series of confocal laser scanning microscope (Olympus, Japan).

In order to detect the apoptosis of neurons, TdT-mediated dUTP Nick-End Labeling (TUNEL) was applied by One-Step TUNEL Assay Kit (Beyotime, China). In a nutshell, after incubating slices with anti-NeuN primary antibody (1:500, Abcam, UK) at 4°C overnight, TUNEL staining was performed in dark for 1 h at 37°C. Finally, DAPI (1:1000, Sigma, USA) staining was proceeded to label cell nucleus. The ratio of apoptotic neurons was calculated by ImageJ software. The percentage of TUNEL-positive neurons (red) compared with total NeuN-stained neurons (green) was used to assess neuron apoptosis. For each sample, four regions were selected for counting, and the average value was calculated.

ELISA assay

LCN2, LDH, IL-1β and IL-18 in astrocytes culture supernatants were measured by ELISA kits according to the manufacturer's instruction (R&D system, USA; Abcam, UK and NEOBIOSCIENCE, China). In short, the sample was added into wells incubated with appropriate antibodies. After the combination between enzyme and substrate, the absorbancy of the samples was detected at 450 nm using a microplate reader (Thermo Fisher Scientific, USA).

Real-time quantitative PCR

Total RNA was extracted by Trizol Reagent (Sigma, USA) from peri-infract region of brains and cultured astrocytes. The extracted RNA was reversely transcribed into cDNA using RevertAid First Strand cDNA Synthesis Kit (Thermo Scientific, USA). A 25 μl reaction system consisted of diluent cDNA (1:10), specific primers and UltraSYBR Mixture (CWBio, China) using Stratagene Mx3000P QPCR system (Agilent Technologies, USA) was performed to proceed real-time quantitative PCR (qPCR). The mRNA expression level of GAPDH was served as endogenous control. The primer pairs used in this research were as follows, 24p3R-forward primer (5-TACCTGATGCGCCTGGAGCT-3), 24p3R-reverse primer (5-TTCTCCAGTTCCTGCAAAGCTT-3); GAPDH-forward primer (5-AAGAAGGTGGTGAAGCAGG-3), GAPDH-reverse primer (5- GAAGGTGGAAGAGTGGGAGT-3).

Transmission electron microscopy

The brain tissues were fixed in electron microscopy fixative solution, processing as mentioned by our previous research [33]. The sections and sheets were scanned by H7500 Transmission Electron Microscope (Hitachi, Japan).

Statistical analysis

Statistical analysis was performed with SPSS software (Vision 22.0, SPSS Inc., IBM, NY, USA). All continuous variables were presented as mean and standard deviation (mean ± S.D.). Two-way repeated-measures ANOVA followed by Tukey's post hoc test was used to analyze mNSS, the escape latecy and swimming pathway in MWM test. Other data were analyzed by one-way ANOVA followed by Tukey's post hoc test. Statistical significance was affirmed by $P < 0.05$.

Results

LCN2 expression in astrocytes is induced by ischemia/reperfusion injury

Reactive astrogliosis occurs after ischemic stroke through a phenomenon of morphological changes and increased expression of GFAP [34]. According to the previous researches, reactive astrogliosis mostly occurs in penumbra region [35, 36]. Our results were consistent with those previous studies (Fig.S1). At 24 h and 72 h post-MCAO surgery, results of IF and WB consistently revealed that GFAP expression was remarkably increased, indicating the activation of astrocytes was mobilized. Co-immunofluorescence staining confirmed that LCN2 expression was triggered by ischemia insults and was well co-localized with GFAP (Fig.1 a, b). LCN2 expression reached a peak at 24 h after MCAO surgery while decreased thereafter (Fig.1 c, d). In *in vitro* model of ischemic stroke, the maximum level of astrocyte LCN2 expression appeared at 12 h after OGD/R (Fig.1 e, f). This was in consistent with ELISA result measuring LCN2 secretion into culture supernatants (Fig.S2 a). LDH release assay demonstrated no significant difference in cell death after reoxygenation for different time periods. The effect of cell activity on the amount of LCN2 release could be ruled out (Fig.S2 b). Therefore, we chose 24 h *in vivo* and 12 h *in vitro* as the optimal time point for the following experiments respectively.

Lcn2 knockout diminishes brain damage and alleviates post-stroke neurological deficits

We applied TTC staining to evaluate infarct volume 24 hours after MCAO. The results demonstrated that infract volume dramatically decreased from 34.40% ± 3.76% to 23.24% ± 4.42% by *Lcn2* gene knockout (Fig.2 a, b; $P < 0.001$). We further investigated whether *Lcn2* deletion could affect ischemia/reperfusion-induced neuronal apoptosis. For this purpose, NeuN/TUNEL co-immunostaining was used to detect the apoptosis of neurons in penumbra (Fig.2 c). There were 50.06% ± 11.66% TUNEL-positive neurons in the peri-infarct region in WT mice. *Lcn2* deletion significantly reduced TUNEL-positive neurons in penumbra to 21.82% ± 3.20% (Fig.2 d, $P < 0.001$).

mNSS was used to assess post-stroke neurological function on post-stroke day 1, 3, 7, 14, 28. As shown in Fig.3 a, mice exposure to MCAO suffered from gradually recovered but permanent sensorimotor deficits. However, *Lcn2* gene deficiency significantly improved post-stroke sensorimotor function compared to WT group ($P < 0.001$ for day 1, 3, 7; $P = 0.007$ for day 14; $P = 0.014$ for day 28). In addition, we used MWM to assess spatial learning and memory function from post-surgery day 22 to 28. With the extension of the training time, the escape latency and path length to the platform were decreased in all groups. Nevertheless, $Lcn2^{-/-}$ mice performed better than WT mice. In the training trial, *Lcn2* deficiency

could reduce escape latency and shorten path length when compared to WT MCAO mice (Fig.3 b, c, $P < 0.001$ for both on the last training day). Probe trail was proceeded the day after the last training day. *Lcn2*$^{-/-}$ mice crossed the hidden platform more times and spent more time in the target quadrant than WT MCAO mice (Fig.3 d-f, $P < 0.05$ for both). No significant differences were observed between the sham-operated groups with either WT or *Lcn2*$^{-/-}$ background.

Lcn2 deficiency alleviates pyroptosis of astrocyte induced by ischemia/reperfusion injury

As GSDMD is the marker of pyroptosis expressed on the membrane, we detected the expression of GSDMD by IF and WB both *in vivo* and *in vitro*. As shown in Fig.4 a, there was scarcely GSDMD expressed in sham-operated groups, but the elevated expression of GSDMD could be induced by MCAO operation. However, GSDMD expression was reduced by *Lcn2* knockout. *In vitro*, we found that GSDMD expressed on the membrane of astrocytes after OGD exposure. *Lcn2*$^{-/-}$ astrocytes showed less GSDMD expression than WT astrocytes (Fig.4 d). The expression of pore-forming protein, GSDMD^{Nterm}, was promoted after ischemia/reperfusion injury, which could be suppressed by *Lcn2* knockout (Fig.4 b, c, e, f, $P < 0.001$ for both *in vivo* and *in vitro*). These results demonstrated that *Lcn2* deficiency could alleviate pyroptosis of astrocyte.

To intuitively observe the pyroptosis pores on astrocytes, microscopic evaluation by electron microscopy was introduced. The GSDMD^{Nterm} formed pores were clearly visible on the membrane of astrocytes suffered from ischemia/reperfusion injury. Membrane pores were less frequent in *Lcn2*$^{-/-}$ group compared to WT group (Fig.4 g). As IL-1β and IL-18 could be released through GSDMD^{Nterm} pores on the membrane of astrocytes [37], we further collected cell culture supernatant to evaluate the efflux of IL-1β and IL-18 in astrocytes. The ELISA assay results suggested that the upregulated secretion of IL-1β and IL-18 were both reversed by *Lcn2* knockout (Fig.4 h, i, $P < 0.001$ for IL-1β and $P = 0.003$ for IL-18).

LCN2 induces NLRP3 inflammasome activation and astrocyte pyroptosis via binding with 24p3R

GSDMD is cleaved to GSDMD^{Nterm} by activated NLRP3 inflammasome, which is essential for the formation of pyroptosis pores [38]. We then investigated whether LCN2 could induce astrocyte pyroptosis through NLRP3 inflammasome activation by IF and WB. As shown in Fig.5, the upregulated expression of the target protein of NLRP3 inflammasome activation pathway, such as ASC, pro-caspase-1, cleaved caspase-1, mature IL-1β and mature IL-18, could be all significantly suppressed by *Lcn2* knockout ($P < 0.001$for all above target protein).

We next asked whether the function of LCN2 on NLRP3 inflammasome was associated with its canonical receptor, 24p3R. By IF, we confirmed that LCN2 and 24p3R were co-localized in astrocytes (Fig.S3). We constructed astrocyte-specific adeno-associated virus-24p3Ri (AAV-GFAP-24p3Ri) to interfere 24p3R expression. Intracerebroventricular injection of AAV-GFAP-GFP and AAV-GFAP-24p3Ri (1.09 E+13 copies/ml, 1.56 E+13 copies/ml, 2 μl) was performed 4 weeks before MCAO surgery (Fig.6 a). We used small animal imaging system and immunostaining of brain sections to confirm that AAV was

successfully injected into lateral ventricle and transfected into astrocytes specifically (Fig.6 b, c). Intracerebroventricular injection of AAV-GFAP-24p3Ri could significantly suppress the expression of 24p3R both in transcriptional and translational level when compared to AAV-GFAP-GFP injection (Fig.6 d-g). The NLRP3 inflammasome activation inducer, 4 mg/kg of Nig, was immediately injected intraperitoneally after MCAO surgery. NLRP3 inflammasome activation was notably enhanced by Nig application (Fig.7 a, b). The results of WB indicated that NLRP3 inflammasome activation and subsequent pyroptosis were inhibited by the interference of 24p3R. The activation of NLRP3 inflammasome by Nig, though, could reverse the 24p3R interference-induced suppression of astrocyte pyroptosis (Fig.7 c, d). Together, these results suggested that the association between LCN2 and 24p3R was necessary in NLRP3 activation-induced astrocyte pyroptosis.

NLRP3 inhibitor abolishes the effects of rLCN2 on astrocyte pyroptosis

We intraperitoneally injected recombinant LCN2 (rLCN2, 10 μl, 10 μg/ml) into

Lcn2$^{-/-}$ mice 5 consecutive days before MCAO surgery. rLCN2 aggravated astrocyte pyroptosis compared to vehicle group. Target protein expression associated with pro-inflammatory cytokines secretion, such as IL-1β and IL-18, were upregulated by rLCN2 induction (Fig.8 a, b). MCC950 is a selective and effective inhibitor of NLRP3 inflammasome. MCC950 (50 μg/kg) was intraperitoneally injected into the mice immediately after MCAO surgery. As expected, MCC950 significantly inhibited NLRP3 inflammasome activation (Fig.8 c, d, $P < 0.001$). The exaggeration on astrocytes pyroptosis induced by rLCN2 was remarkably reversed by MCC950. All these results reproducibly suggested that LCN2/24p3R mediated pyroptosis of astrocytes via NLRP3 inflammasome after cerebral ischemia/reperfusion injury. Meanwhile, restraining astrocyte pyroptosis could lighten neurological impairment (Fig.8 e).

Discussion

The present study identifies LCN2 as an important regulator in astrocyte pyroptosis following cerebral ischemia/reperfusion injury. LCN2 was increased in astrocytes of peri-infarction area after MCAO. Genetic knockout of *Lcn2* could improve short-term and long-term outcomes of MCAO mice. Mechanistically, we verified co-localization of LCN2 and 24p3R in astrocytes, providing a physical basis for their association. Pyroptosis of astrocytes was alleviated using astrocyte-specific AAV-GFAP-24p3Ri, which could be reversed by NLRP3 inflammasome activator. Likewise, re-expression of LCN2 in *Lcn2*$^{-/-}$ mice aggravated GSDMD-mediated pyroptosis. This detrimental effect could be mitigated by 24p3R interference or NLRP3 inhibition. Collectively, in cerebral ischemia/reperfusion injury, LCN2 can bind to the 24p3R on astrocytes membrane and facilitate NLRP3 activation, which can ultimately trigger astrocyte pyroptosis and pro-inflammatory effects (Fig. 10). This research provides new insights into the important role of LCN2 in neuroinflammation after cerebral ischemia.

It has been widely accepted that neuroinflammation is a vital secondary injury following stroke. It is recently discovered that the multiprotein complexes termed “inflammasomes”, firstly described by

Martinon [39], were involved in the initiation of inflammatory response [40]. Inflammasomes generally are consisted of three components: a cytosolic pattern-recognition pattern (PRP) sensing damage-associated molecular patterns (DAMPs) released from the dead cells, the caspase-1 protease and an adaptor protein facilitates integrating the two components [41]. So far, the inflammasomes NLRC4, NLRP1, NLPR3, NLRP6 and AIM have been implicated in ischemic stroke [12, 13, 42]. Among them NLRP3 inflammasome is the most well-studied regulator of caspase-1 activation related to sterile inflammation in neurological diseases [43, 44]. NLRP3 protein was found to be increased following ischemic stroke. Inhibiting NLRP3 inflammasome activation could improve neurological function [45, 46]. Some research suggested that NLRP3 transcript was not apparently expressed in astrocytes at baseline but could be induced by NLRP3-activation stimuli, such as recombinant Aβ [47]. NLRP3 inflammasome activation could initiate pro-inflammatory programmed cell death, termed pyroptosis [48].In brief, DAMPs released from damaged cells are recognized by pattern recognition receptor (PRR) to stimulate NLRP3 inflammasome activation, followed by pro-caspase-1 mature promoting. Gasdermins are the executor of pyroptosis, represented by GSDMD [49]. Caspase-1 cleaves full-length GSDMD into $GSDMD^{Nterm}$, polymerization of $GSDMD^{Nterm}$ forms the characteristic membrane pores of pyroptosis (Aglietti and Dueber, 2017; Ding et al., 2016; Liu et al., 2016; Sborgi et al., 2016). However, the triggers of NLRP3 inflammasome activation in ischemic stroke remains unclear. Activated astrocytes following ischemic stroke could respond to inflammatory signals and promote inflammation. Nowadays, mounting evidences demonstrated that pyroptosis of astrocytes was involved in cerebral ischemia/reperfusion pathologic process. Suppressing NLRP3-mediated pyroptosis of astrocytes by hispidulin could improve neurological symptoms and decrease pro-inflammatory cytokines secretion, infract volume and brain edema [11]. Pioglitazone conferred neuroprotective function against astrocyte pyroptosis in brain injury [10]. Our results substantiated that NLRP3 inflammasome was activated in astrocytes and subsequently caused astrocyte pyroptosis during ischemic stroke. Once NLRP3 activation was inhibited, the pyroptosis of astrocytes was suppressed, suggesting that NLRP3 initiation was necessary in astrocyte pyroptosis following cerebral ischemia/reperfusion injury.

Lipocalin-2 (LCN2) is an acute phase protein and mainly secreted from activated astrocytes under diverse brain injury conditions [16]. LCN2 acts as an autocrine pattern on astrocyte. To date, studies about the role of LCN2 on astrocyte mainly focused on reactive astrocytosis. Astrocyte has two distinct activation phenotypes, classic activation (pro-inflammatory one) and alternative activation (anti-inflammatory one). LCN2 auto-secreted from activated astrocytes could in turn stimulate the classic activation and provide inflammation-promoting function [18, 50]. Our previous study also proved the necessity of LCN2 for astrocyte classic activation using $Lcn2^{-/-}$ mice [19]. Devireddy documented that LCN2 could mediate cell apoptosis via binding with 24p3R [51]. We further expanded the function of LCN2/24p3R to cell pyroptosis. We found that LCN2 could trigger pyroptosis of astrocyte via binding with 24p3R, and the generation of pro-inflammatory cytokines and neurologic impairment was alleviated by *Lcn2* gene knockout. LCN2 can amplify inflammasome through astrocytes/microglia activation and neutrophil infiltration [21]. Even LCN2 may have direct neurotoxic effect by binding with receptor on neurons [20]. Our study found that LCN2-mediated astrocytic pyroptosis could cause neuron damage. Here we

discussed the possible mechanisms for further study. Astrocyte-neuron crosstalk contributes to the pathological process of various neurological diseases, and neurotoxic effects of activated astrocytes have been widely studied.[52–54]. Among them, the study about effect of astrocytic pyroptosis on neurons are attracting more and more attention. In a sepsis model, pyroptosis of astrocytes caused increased release of pro-inflammatory cytokines (IL-1β and IL-18), resulting neuron damage[55]. Another study found that pyroptosis, especially occurred in astrocytes, promoted disruption of blood-brain barrier integrity and accumulation of toxic Aβ, ultimately leading to neuronal death after I/R injury[56]. Another *in vitro* study demonstrated that pyroptosis of astrocytes decreased neuronal viability and aggravated neuronal apoptosis through caspase-1 activation[13]. Refer to the above, aggravated neuroinflammation and neuronal damage may lead to increased infract volume by MCAO.

In summary, our data support a pro-pyroptotic role of LCN2 in cerebral ischemia/reperfusion injury. Inhibiting LCN2-induced astrocyte pyroptosis may be a promising therapeutic target for ischemia stroke management.

Abbreviations

LCN2 Lipocalin-2

MCAO Middle cerebral artery occlusion

O/R Oxygen-glucose deprivation and reoxygenation

AAV-GFAP-24p3Ri astrocyte-specific adeno-associated virus

Nig Nigericin sodium salt

rLCN2 Recombinant lipocalin-2

CCA Common carotid artery

ECA External carotid artery

ICA Internal carotid artery

MCA Middle cerebral artery

TTC 2,3,5- triphenyltetrazoliumchloride

PFA Paraformaldehyde

mNSS the Modified Neurologic Severity Score

MWM Morris Water Maze

AAV Adeno-associated virus

Nig Nigericin sodium salt

HBSS Hank’s balanced salt solution

DMEM Dulbecco’s Modified Eagle Medium

PDL Poly-D-Lysine

PBS Phosphate buffer saline

OGD Oxygen-glucose deprivation

WB Western blotting

SDS-PAGE Sodium dodecyl sulfate-polyacrylamide gel electrophoresis

PVDF Polyvinylidene difluoride

IF Immunofluorescence

BSA Bovine serum albumin

TUNEL TdT-mediated dUTP Nick-End Labeling

qPCR Real-time quantitative PCR
AAV-GFAP-24p3Ri Astrocyte-specific adeno-associated virus-24p3Ri

PRP Pattern-recognition pattern

DAMPs Damage-associated molecular patterns

PRR Pattern recognition receptor

Declarations

Ethical Approval and Consent to participate

All the experiments involving animals were approved by Experimental Animal Ethics Committee of Jinling Hospital. All experimental protocols were performed in accordance with the National Institutes of Health “Guide for the Care and Use of Laboratory Animals” (NIH Publications no. 8023, revised 2011).

Consent for publication

Not applicable.

Availability of data and materials

The data that support the findings of this study are available from the corresponding author upon reasonable request.

Competing interests

The authors declare no financial or otherwise conflicts of interest.

Funding

This work was supported by the National Key Research and Development Program Project of China (No. 2017YFC1307901), the National Natural Science Foundation of China (No. U20A20357), Natural Science Foundation of Jiangsu Province (No. BK20201234); Natural Science Foundation of Anhui Province (No. 2008085QH368).

Authors' contributions

Juanji Li, Pengfei Xu and Ye Hong contributed equally to this work. Juanji Li and Pengfei Xu wrote the main manuscript text. Most of in vivo and vitro experiments were completed by Juanji Li. Ye Hong and Rui Sun were in charge of establishing MCAO model. Yi Xie, Xiaohao Zhang and Mengna Peng raised Lcn2 gene knockout mice. Wusheng Zhu, Junjun Wang and Xinfeng Liu guided the project design and the manuscript writing. All authors reviewed the maunuscript.

References

1. Shi, K., et al., *Global brain inflammation in stroke.* Lancet Neurol, 2019. **18**(11): p. 1058-1066.
2. Sofroniew, M.V., *Astrocyte barriers to neurotoxic inflammation.* Nat Rev Neurosci, 2015. **16**(5): p. 249-63.
3. Hu, X., et al., *Microglial and macrophage polarization—new prospects for brain repair.* Nat Rev Neurol, 2015. **11**(1): p. 56-64.
4. Lan, X., et al., *Modulators of microglial activation and polarization after intracerebral haemorrhage.* Nat Rev Neurol, 2017. **13**(7): p. 420-433.
5. Liddelow, S.A. and B.A. Barres, *Reactive Astrocytes: Production, Function, and Therapeutic Potential.* Immunity, 2017. **46**(6): p. 957-967.
6. Li, M., et al., *Astrocyte-derived interleukin-15 exacerbates ischemic brain injury via propagation of cellular immunity.* Proc Natl Acad Sci U S A, 2017. **114**(3): p. E396-e405.
7. Wilson, E.H., W. Weninger, and C.A. Hunter, *Trafficking of immune cells in the central nervous system.* J Clin Invest, 2010. **120**(5): p. 1368-79.
8. Shi, J., W. Gao, and F. Shao, *Pyroptosis: Gasdermin-Mediated Programmed Necrotic Cell Death.* Trends Biochem Sci, 2017. **42**(4): p. 245-254.

9. Sborgi, L., et al., *GSDMD membrane pore formation constitutes the mechanism of pyroptotic cell death.* Embo j, 2016. **35**(16): p. 1766-78.
10. Xia, P., et al., *Pioglitazone Confers Neuroprotection Against Ischemia-Induced Pyroptosis due to its Inhibitory Effects on HMGB-1/RAGE and Rac1/ROS Pathway by Activating PPAR- .* Cell Physiol Biochem, 2018. **45**(6): p. 2351-2368.
11. An, P., et al., *Hispidulin exhibits neuroprotective activities against cerebral ischemia reperfusion injury through suppressing NLRP3-mediated pyroptosis.* Life Sci, 2019. **232**: p. 116599.
12. Meng, C., et al., *Effects of NLRP6 in Cerebral Ischemia/Reperfusion (I/R) Injury in Rats.* J Mol Neurosci, 2019. **69**(3): p. 411-418.
13. Zhang, J., et al., *NLRP6 expressed in astrocytes aggravates neurons injury after OGD/R through activating the inflammasome and inducing pyroptosis.* Int Immunopharmacol, 2020. **80**: p. 106183.
14. Flower, D.R., *The lipocalin protein family: a role in cell regulation.* FEBS Lett, 1994. **354**(1): p. 7-11.
15. Ferreira, A.C., et al., *From the periphery to the brain: Lipocalin-2, a friend or foe?* Prog Neurobiol, 2015. **131**: p. 120-36.
16. Jha, M.K., et al., *Diverse functional roles of lipocalin-2 in the central nervous system.* Neurosci Biobehav Rev, 2015. **49**: p. 135-56.
17. Lee, S., et al., *A dual role of lipocalin 2 in the apoptosis and deramification of activated microglia.* J Immunol, 2007. **179**(5): p. 3231-41.
18. Lee, S., et al., *Lipocalin-2 is an autocrine mediator of reactive astrocytosis.* J Neurosci, 2009. **29**(1): p. 234-49.
19. Zhao, N., et al., *Lipocalin-2 may produce damaging effect after cerebral ischemia by inducing astrocytes classical activation.* J Neuroinflammation, 2019. **16**(1): p. 168.
20. Jin, M., et al., *Lipocalin-2 deficiency attenuates neuroinflammation and brain injury after transient middle cerebral artery occlusion in mice.* J Cereb Blood Flow Metab, 2014. **34**(8): p. 1306-14.
21. Suk, K., *Lipocalin-2 as a therapeutic target for brain injury: An astrocentric perspective.* Prog Neurobiol, 2016. **144**: p. 158-72.
22. Kehrer, J.P., *Lipocalin-2: pro- or anti-apoptotic?* Cell Biol Toxicol, 2010. **26**(2): p. 83-9.
23. Sung, H.K., et al., *Lipocalin-2 (NGAL) Attenuates Autophagy to Exacerbate Cardiac Apoptosis Induced by Myocardial Ischemia.* J Cell Physiol, 2017. **232**(8): p. 2125-2134.
24. Poh, L., et al., *Evidence that NLRC4 inflammasome mediates apoptotic and pyroptotic microglial death following ischemic stroke.* Brain Behav Immun, 2019. **75**: p. 34-47.
25. Xu, P., et al., *Breast cancer susceptibility protein 1 (BRCA1) rescues neurons from cerebral ischemia/reperfusion injury through NRF2-mediated antioxidant pathway.* Redox Biol, 2018. **18**: p. 158-172.
26. Sun, R., et al., *Low-density lipoprotein receptor (LDLR) regulates NLRP3-mediated neuronal pyroptosis following cerebral ischemia/reperfusion injury.* J Neuroinflammation, 2020. **17**(1): p. 330.

27. Xie, Y., et al., *Human Albumin Improves Long-Term Behavioral Sequelae After Subarachnoid Hemorrhage Through Neurovascular Remodeling.* Crit Care Med, 2015. **43**(10): p. e440-9.
28. Kim, J.H., et al., *Astrocyte-derived lipocalin-2 mediates hippocampal damage and cognitive deficits in experimental models of vascular dementia.* Glia, 2017. **65**(9): p. 1471-1490.
29. Deng, C.C., et al., *Nigericin selectively targets cancer stem cells in nasopharyngeal carcinoma.* Int J Biochem Cell Biol, 2013. **45**(9): p. 1997-2006.
30. Sui, A., et al., *Inhibiting the NLRP3 inflammasome with MCC950 ameliorates retinal neovascularization and leakage by reversing the IL-1β/IL-18 activation pattern in an oxygen-induced ischemic retinopathy mouse model.* Cell Death Dis, 2020. **11**(10): p. 901.
31. Hong, Y., et al., *High-frequency repetitive transcranial magnetic stimulation improves functional recovery by inhibiting neurotoxic polarization of astrocytes in ischemic rats.* J Neuroinflammation, 2020. **17**(1): p. 150.
32. Ye, R., et al., *Sevoflurane preconditioning improves mitochondrial function and long-term neurologic sequelae after transient cerebral ischemia: role of mitochondrial permeability transition.* Crit Care Med, 2012. **40**(9): p. 2685-93.
33. Xie, Y., et al., *Aberrant oligodendroglial LDL receptor orchestrates demyelination in chronic cerebral ischemia.* J Clin Invest, 2021. **131**(1).
34. Choudhury, G.R. and S. Ding, *Reactive astrocytes and therapeutic potential in focal ischemic stroke.* Neurobiol Dis, 2016. **85**: p. 234-244.
35. Hayakawa, K., et al., *Inhibition of reactive astrocytes with fluorocitrate retards neurovascular remodeling and recovery after focal cerebral ischemia in mice.* J Cereb Blood Flow Metab, 2010. **30**(4): p. 871-82.
36. Shimada, I.S., et al., *Proliferating reactive astrocytes are regulated by Notch-1 in the peri-infarct area after stroke.* Stroke, 2011. **42**(11): p. 3231-7.
37. Broz, P., P. Pelegrín, and F. Shao, *The gasdermins, a protein family executing cell death and inflammation.* Nat Rev Immunol, 2020. **20**(3): p. 143-157.
38. Gaidt, M.M. and V. Hornung, *Pore formation by GSDMD is the effector mechanism of pyroptosis.* Embo j, 2016. **35**(20): p. 2167-2169.
39. Martinon, F., K. Burns, and J. Tschopp, *The inflammasome: a molecular platform triggering activation of inflammatory caspases and processing of proIL-beta.* Mol Cell, 2002. **10**(2): p. 417-26.
40. Walsh, J.G., D.A. Muruve, and C. Power, *Inflammasomes in the CNS.* Nat Rev Neurosci, 2014. **15**(2): p. 84-97.
41. Schroder, K. and J. Tschopp, *The inflammasomes.* Cell, 2010. **140**(6): p. 821-32.
42. Voet, S., et al., *Inflammasomes in neuroinflammatory and neurodegenerative diseases.* EMBO Mol Med, 2019. **11**(6).
43. Cassel, S.L. and F.S. Sutterwala, *Sterile inflammatory responses mediated by the NLRP3 inflammasome.* Eur J Immunol, 2010. **40**(3): p. 607-11.

44. Feng, Y.S., et al., *Inhibition of NLRP3 Inflammasome: A Prospective Target for the Treatment of Ischemic Stroke.* Front Cell Neurosci, 2020. **14**: p. 155.
45. Fann, D.Y., et al., *Intravenous immunoglobulin suppresses NLRP1 and NLRP3 inflammasome-mediated neuronal death in ischemic stroke.* Cell Death Dis, 2013. **4**(9): p. e790.
46. Yang, F., et al., *NLRP3 deficiency ameliorates neurovascular damage in experimental ischemic stroke.* J Cereb Blood Flow Metab, 2014. **34**(4): p. 660-7.
47. Ebrahimi, T., et al., *α1-antitrypsin mitigates NLRP3-inflammasome activation in amyloid β(1-42)-stimulated murine astrocytes.* J Neuroinflammation, 2018. **15**(1): p. 282.
48. Bergsbaken, T., S.L. Fink, and B.T. Cookson, *Pyroptosis: host cell death and inflammation.* Nat Rev Microbiol, 2009. **7**(2): p. 99-109.
49. McKenzie, B.A., V.M. Dixit, and C. Power, *Fiery Cell Death: Pyroptosis in the Central Nervous System.* Trends Neurosci, 2020. **43**(1): p. 55-73.
50. Jang, E., et al., *Phenotypic polarization of activated astrocytes: the critical role of lipocalin-2 in the classical inflammatory activation of astrocytes.* J Immunol, 2013. **191**(10): p. 5204-19.
51. Devireddy, L.R., et al., *A cell-surface receptor for lipocalin 24p3 selectively mediates apoptosis and iron uptake.* Cell, 2005. **123**(7): p. 1293-305.
52. Liddelow, S.A., et al., *Neurotoxic reactive astrocytes are induced by activated microglia.* Nature, 2017. **541**(7638): p. 481-487.
53. Wheeler, M.A., et al., *MAFG-driven astrocytes promote CNS inflammation.* Nature, 2020. **578**(7796): p. 593-599.
54. Zamanian, J.L., et al., *Genomic analysis of reactive astrogliosis.* J Neurosci, 2012. **32**(18): p. 6391-410.
55. Sun, Y.B., et al., *Dexmedetomidine inhibits astrocyte pyroptosis and subsequently protects the brain in in vitro and in vivo models of sepsis.* Cell Death Dis, 2019. **10**(3): p. 167.
56. Lyu, Z., et al., *Destructive Effects of Pyroptosis on Homeostasis of Neuron Survival Associated with the Dysfunctional BBB-Glymphatic System and Amyloid-Beta Accumulation after Cerebral Ischemia/Reperfusion in Rats.* Neural Plast, 2021. **2021**: p. 4504363.

Figures

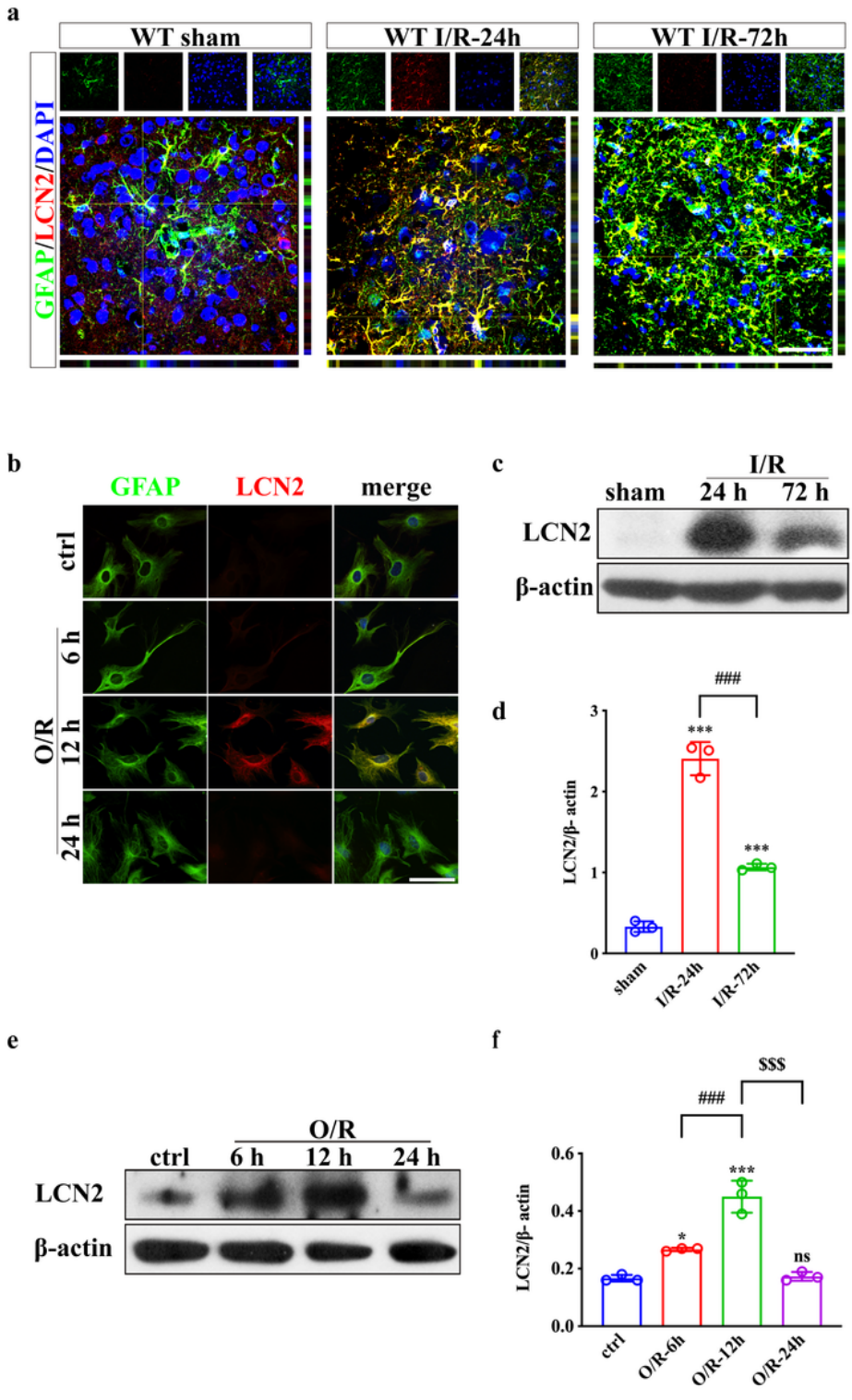

Figure 1

The LCN2 expression in astrocytes was upregulated following ischemia/reperfusion injury both *in vivo* and *in vitro*. (a, b) Double label immunofluorescence staining for GFAP (green) and LCN2 (red) in peri-infract region and OGD/R treated astrocytes. Scale bar = 20 μm. **(c-f)** Immunoblotting analysis of LCN2 expression after MCAO or OGD/R. All data were shown as mean ± S.D.; n = 3 per group; $^{***}P < 0.001$, $^{*}P < 0.05$ versus sham-operated group or control group; $^{\#\#\#}P < 0.001$, $^{\$\$\$}P < 0.001$.

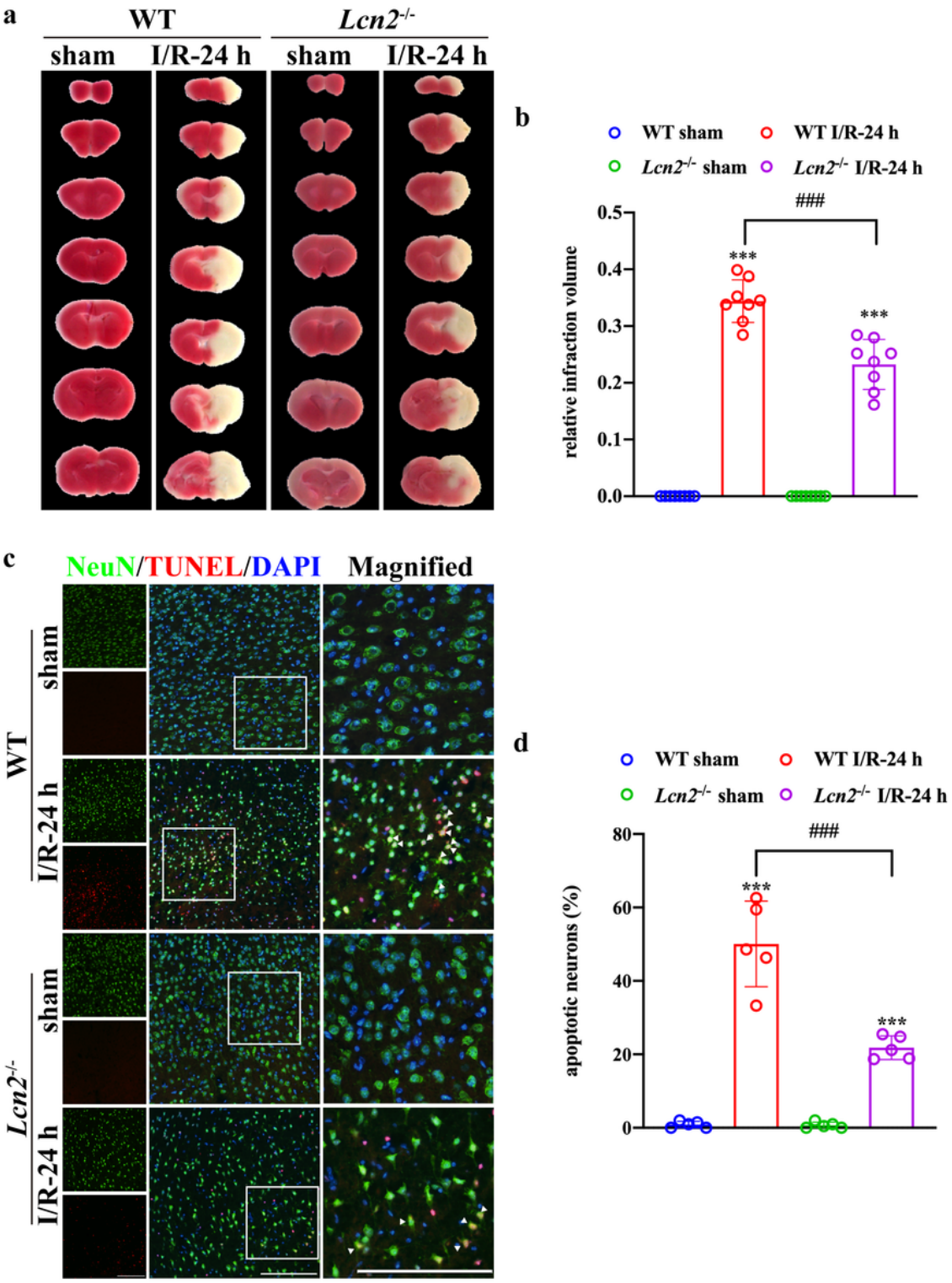

Figure 2

***Lcn2* knockout reduces infract volume and neuronal death after MCAO surgery. (a, b)** Infract volume was assessed by TTC (2, 3, 5-triphenyltetrazoliumchloride) staining 24 h after MCAO surgery. n = 10 per group. **(c, d)** Presentative images of double staining of TUNEL (red) with NeuN (green) to assess the proportion of apoptotic neurons after MCAO surgery. Scale bar = 50 μm. All data were shown as mean ± S.D.; $^{***}P < 0.001$ versus corresponding sham-operated group; $^{###}P < 0.001$.

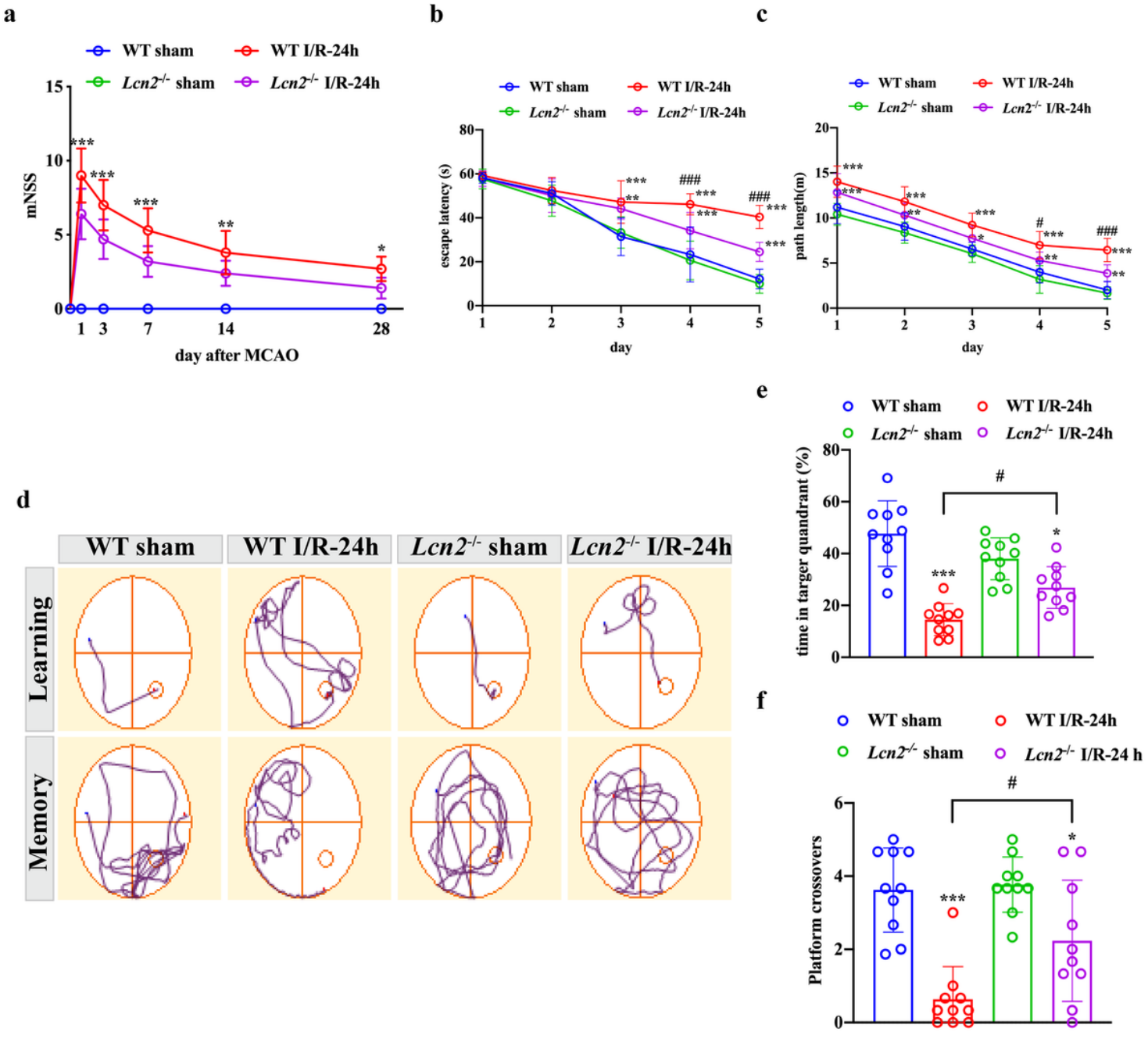

Figure 3

***Lcn2* deletion alleviates post-stroke neurological deficits. (a)** mNSS were used for sensorimotor function assessment after MCAO surgery. $^{***}P < 0.001$, $^{**}P < 0.01$, $^{*}P < 0.05$ for MCAO-operated mice in WT group versus *Lcn2*$^{-/-}$ group. **(b-f)** Long-term cognitive function was assessed by MWM (Morris Water Maze) test at day 22-28 post MCAO surgery. **(d)** Representative swimming path trace of mice attempting to find the hidden platform on the last training day (top traces, "learning"), or searching for the removed platform in the probe trail (below traces, "memory"). **(b, c)** Escape latency and path length were recorded on day 23-27 post-MCAO surgery. $^{***}P < 0.001$, $^{**}P < 0.01$, $^{*}P < 0.05$ for MCAO-operated group versus corresponding sham-operated group; $^{\#\#\#}P < 0.001$, $^{\#}P < 0.05$ for MCAO-operated mice in WT group versus LCN2$^{-/-}$ group.

(e, f) Time in target quadrant and platform crossovers were recorded in the probe trail, $^{***}P < 0.001$ and $^{*}P < 0.05$ for MCAO-operated group versus corresponding sham-operated group; $^{\#}P < 0.05$. All data were shown as mean ± S.D.; n = 10 per group.

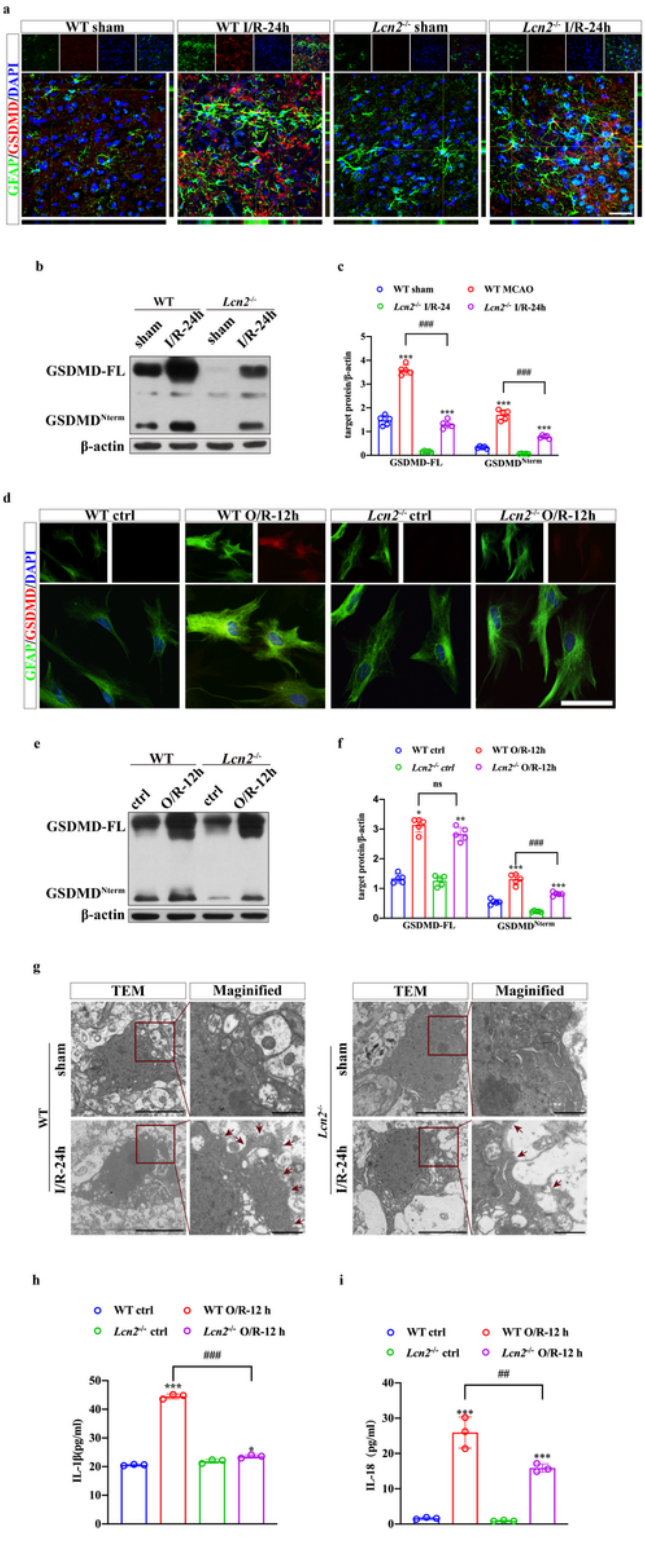

Figure 4

***Lcn2* deficiency alleviates pyroptosis of astrocyte induced by ischemia/reperfusion injury. (a, d)** Double-label immunofluorescence staining for GFAP (green) and GSDMD (red) *in vivo* and *in vitro*. Scale bar = 20 μm. **(b, c, e, f)** WB analysis of GSDMD protein expression in penumbra tissue and cultured astrocytes. All data were shown as mean ± S.D.; n = 5 per group; $^{***}P < 0.001$, $^{**}P < 0.01$, $^{*}P < 0.05$ for MCAO-operated group versus corresponding sham-operated group or OGD/R-cells versus corresponding control cells; $^{###}P < 0.001$. **(g)** Representative image of TEM of astrocytes in peri-infract brain tissue. The red arrows pointed to pyroptosis pores on the cell membrane. Scale bar = 5 μm and 1 μm for magnified image. **(h, i)** IL-1β and IL-18 secretion into supernatants measured by ELISA kits. All data were shown as mean ± S.D.; n = 3 per group; $^{***}P < 0.001$ for OGD/R-cells versus corresponding control cells; $^{###}P < 0.001$, $^{##}P < 0.01$.

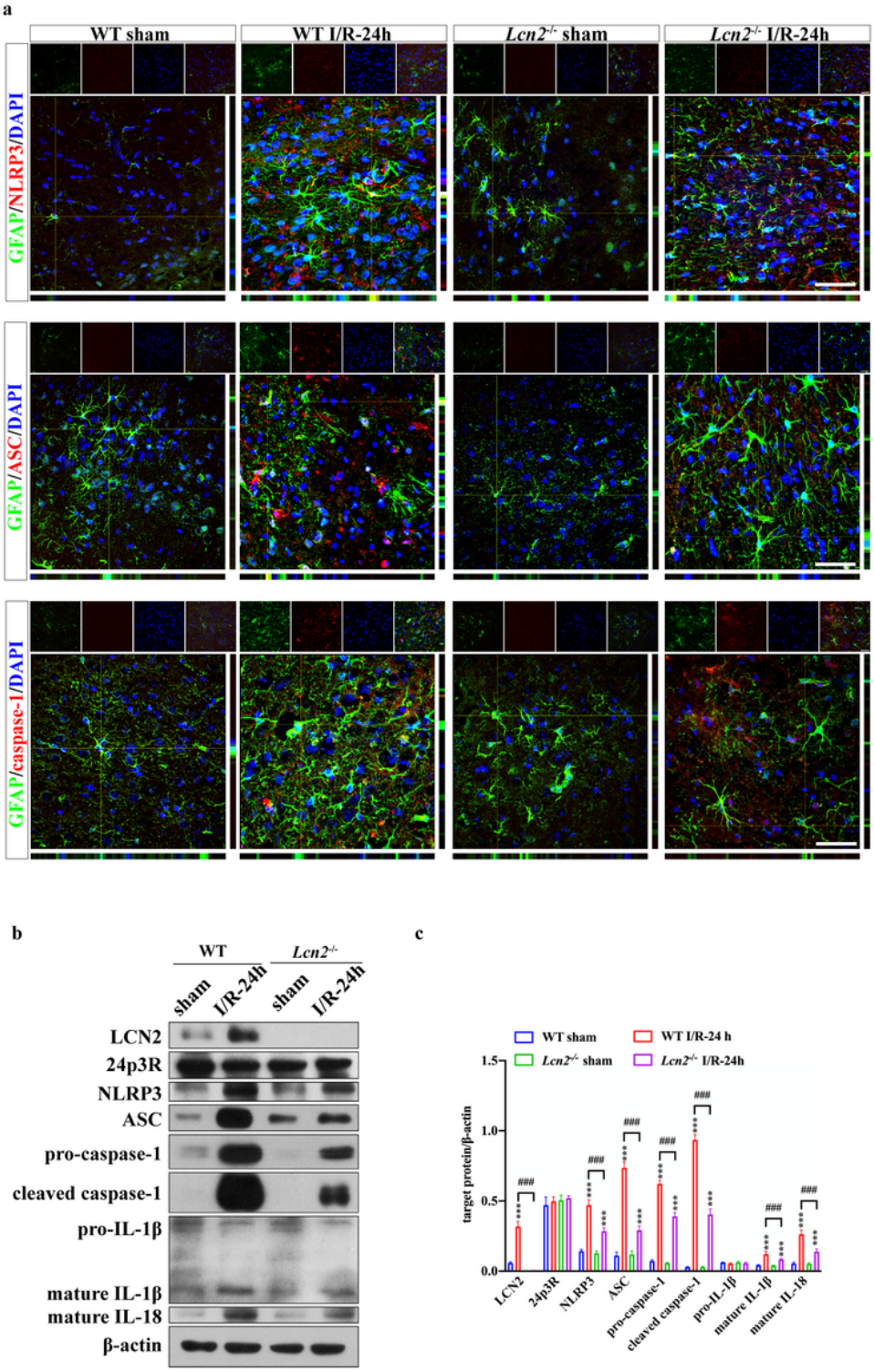

Figure 5

LCN2 induces NLRP3 inflammasome activation and subsequent pyroptosis in astrocytes. (a) Co-immunofluorescence staining of GFAP with NLRP3, ASC, and caspase-1. Scale bar = 20 μm. **(b)**WB analysis of expression of LCN2, 24p3R, NLRP3, ASC, pro-caspase-1, cleaved caspase-1, pro-IL-1β, mature IL-1β, mature IL-18 in penumbra region. All data were shown as mean ± S.D.; n = 5 per group; $^{***}P < 0.001$ versus corresponding sham-operated group; $^{###}P < 0.001$.

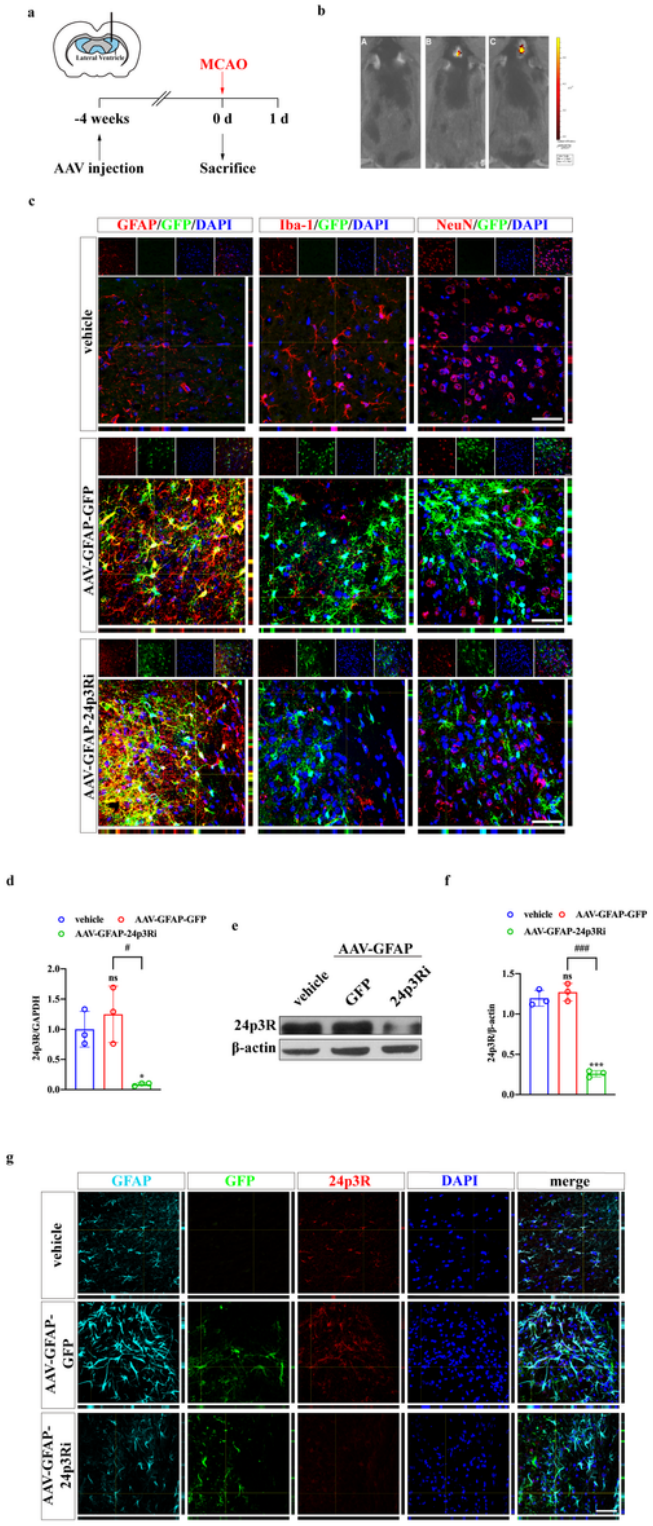

Figure 6

AAV-GFAP-24p3Ri transfection reduces 24p3R expression in astrocyte. (a) Schematic diagram of intracerebroventricular injection procedure. **(b)** Representative images of small animal imaging system. A. WT MCAO-operated mouse; B. WT MCAO-operated mouse with AAV-GFAP-GFP injection; C. WT MCAO-

operated mouse with AAV-GFAP-24p3Ri injection. **(c)** Representative images of AAV (labeled with GFP, green) specifically transfected into astrocytes but not microglia and neurons (labeled with GFAP, Iba-1, and NeuN, red). Scale bar = 20 μm. **(d)** qPCR was used to verify the efficacy of 24p3Ri in transcriptional level. n = 3 per group; $^{*}P < 0.05$ versus vehicle-injection group; $^{\#}P < 0.5$. **(e, f)** Detection of interference of 24p3R expression in translational level by WB. n = 3 per group; $^{***}P < 0.01$ versus vehicle-injection group; $^{\#\#\#}P < 0.001$. **(g)** IF showed that astrocytic-24p3R expression was significantly inhibited by AAV-GFAP-24p3Ri injection. Scale bar = 20 μm.

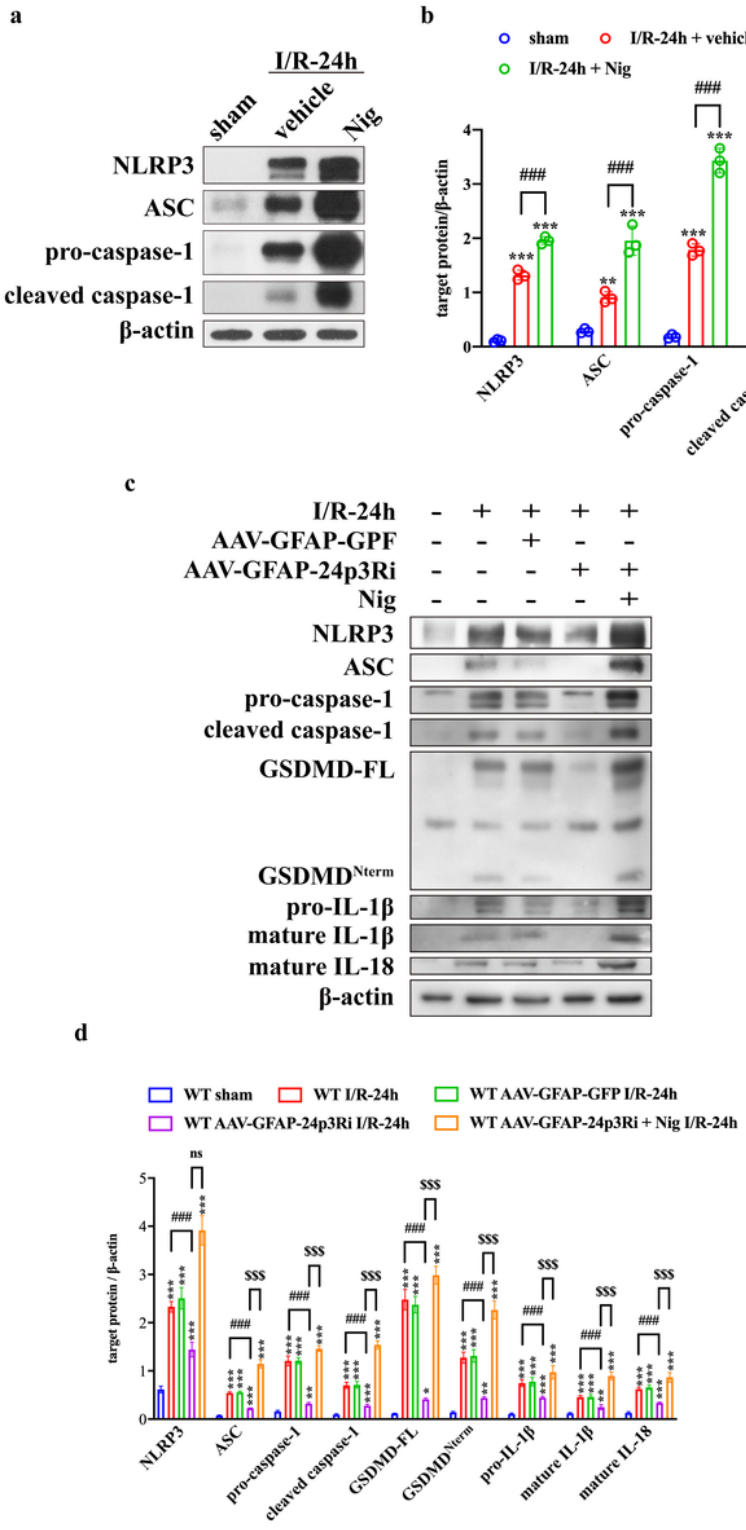

Figure 7

LCN2 mediates astrocyte pyroptosis by NLRP3 inflammasome activation via binding to 24p3R. (a, b) The efficacy of Nig to induce NLRP3 inflammasome activation was evaluated by WB. n = 3 per group; $^{***}P < 0.001$, $^{**}P < 0.01$; $^{*}P < 0.05$ versus sham-operated group; $^{###}P < 0.001$. **(c, d)** WB analysis of NLRP3, ASC, pro-caspase-1, cleaved caspase-1, GSDMD-FL, $GSDMD^{Nterm}$, pro-IL-1β, mature IL-1β, mature IL-18. n = 5

per group; $^{***}P < 0.001$, $^{**}P < 0.01$ versus sham-operated group; $^{###}P < 0.001$; $^{$$$}P < 0.001$. All data were shown as mean ± S.D..

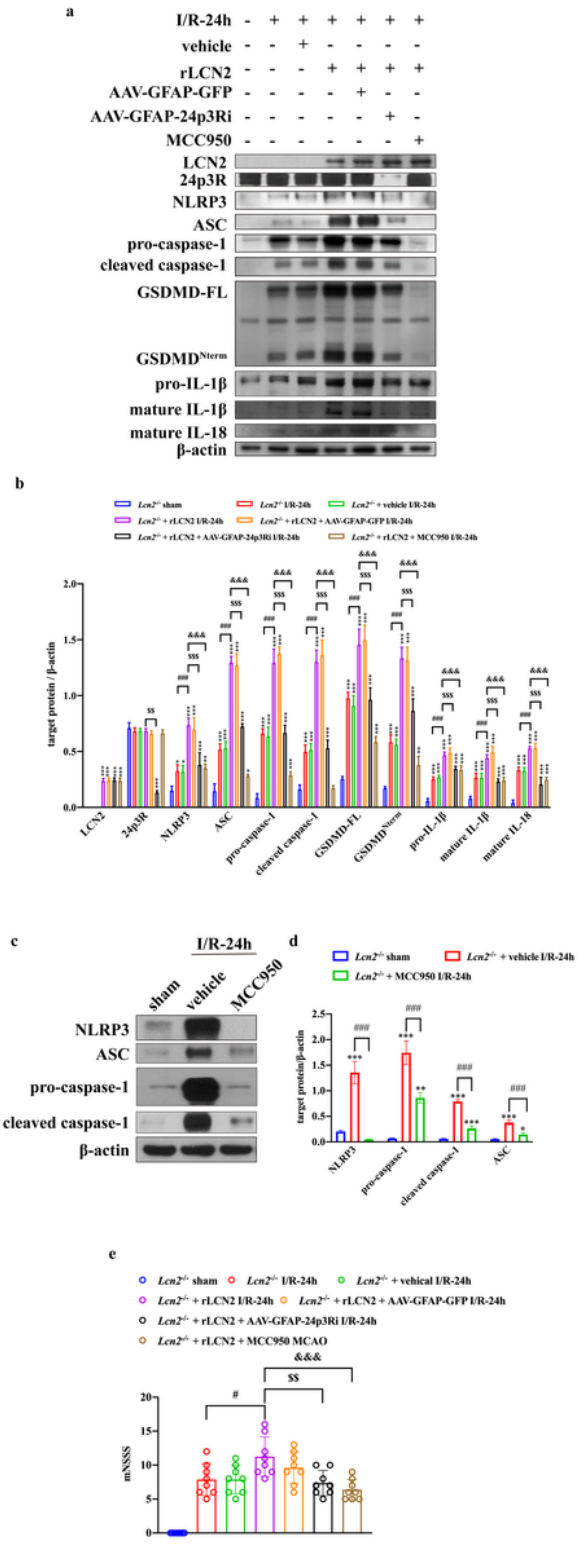

Figure 8

NLRP3 inhibitor abolished detrimental effects of rLCN2 on pyroptosis and functional prognosis. (a, b) WB analysis of LCN2, 24p3R and target protein in NLRP3 inflammasome and pyroptosis pathway. n = 5 per

group; $^{***}P < 0.001$, $^{**}P < 0.01$, $^{*}P < 0.05$ versus sham-operated group; $^{\#\#\#}P < 0.001$; $^{\$\$\$}P < 0.001$, $^{\$\$}P < 0.01$; $^{\&\&\&}P < 0.001$. **(c, d)** Detection of MCC950 function by WB analysis of NLRP3 expression. n = 3 per group; $^{***}P < 0.001$, $^{**}P < 0.01$, $^{*}P < 0.05$ versus sham-operated group; $^{\#\#\#}P < 0.001$. **(e)** Neurologic impairment assessment on 24 h after MCAO surgery. n = 8 per group; $^{\#}P < 0.05$; $^{\$\$}P < 0.01$; $^{\&\&\&}P < 0.001$. All data were presented as mean ± S.D..

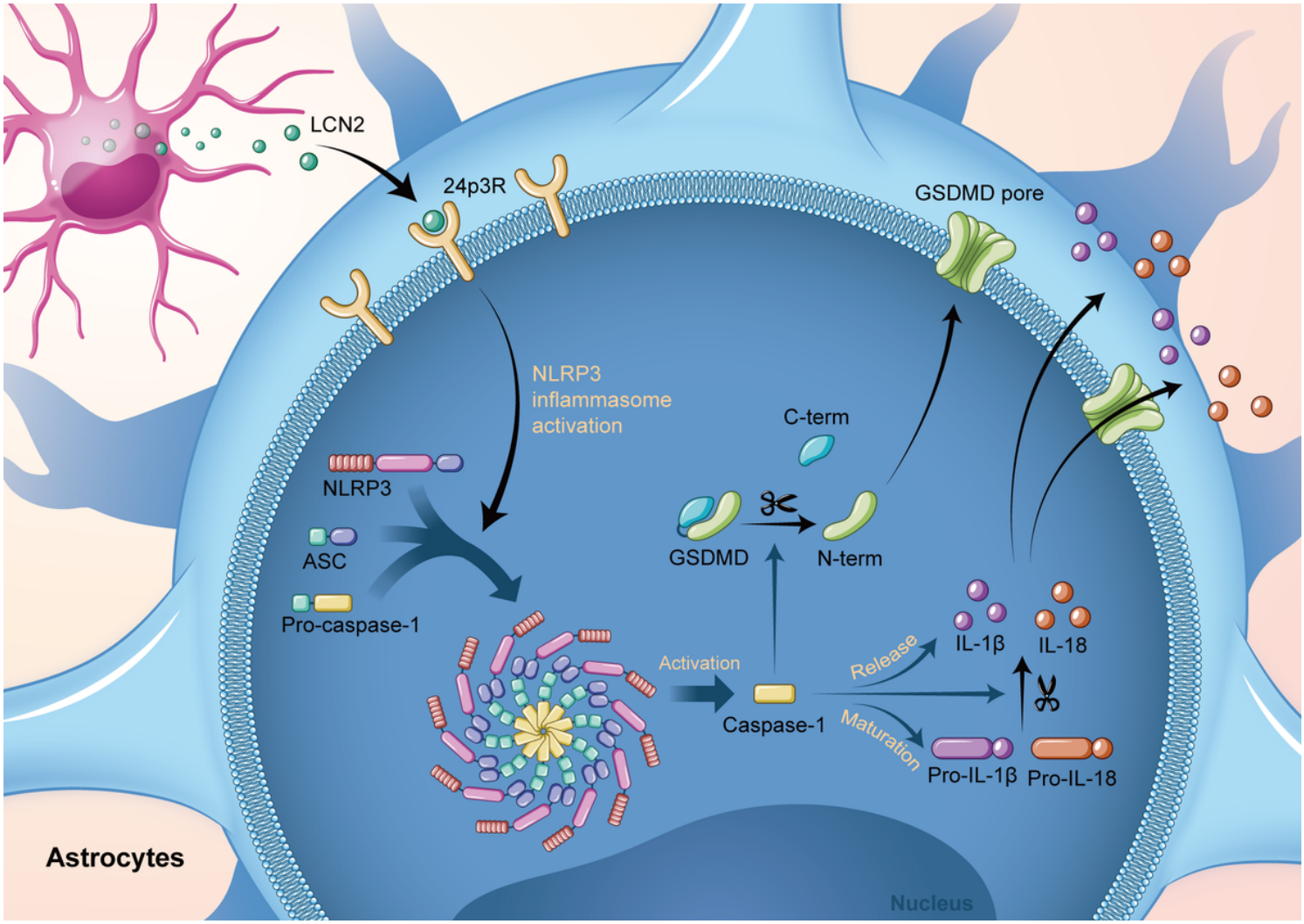

Figure 9

LCN2, secreted from astrocytes during brain ischemia/reperfusion injury, binded to 24p3R on the membrane of astrocytes. This process could stimulate the activation of NLRP3 inflammasome. Pro-caspase-1 was subsequently cleaved into caspase-1. $GSDMD^{Nterm}$ cleaved by caspase-1 polymerized on the cell membrane forming $GSDMD^{Nterm}$ pores and caused programmed inflammatory cell death, pyroptosis. Activated caspase-1 could also promote the maturation and release of pro-inflammatory cytokines such as IL-1β and IL-18.

Supplementary Files

This is a list of supplementary files associated with this preprint. Click to download.

- Fig.S1bGFAP.tif
- Fig.S1bactin.tif
- Fig.4bGSDMD.tif
- Fig.4bactin.tif
- Fig.4eGSDMD.tif
- Fig.4eactin.tif
- Fig.524p3R.tif
- Fig.5ASC.tif
- Fig.5IL18.tif
- Fig.5IL1.tif
- Fig.5LCN2.tif
- Fig.5NLRP3.tif
- Fig.5caspase1.tif
- Fig.5actin.tif
- Fig.6e24p3R.tif
- Fig.6eactin.tif
- Fig.7aASC.tif
- Fig.7aNLRP3.tif
- Fig.7acaspase1.tif
- Fig.7aactin.tif
- Fig.7cASC.tif
- Fig.7cGSDMD.tif
- Fig.7cIL18.tif
- Fig.7cIL1.tif
- Fig.7cNLRP3.tif
- Fig.7ccaspase1.tif
- Fig.7cactin.tif
- Fig.8a24p3R.tif
- Fig.8aASC.tif
- Fig.8aGSDMD.tif
- Fig.8aIL1.tif
- Fig.8aLCN2.tif
- Fig.8aNLRP3.tif

- Fig.8acaspase1.tif
- Fig.8aactin.tif
- Fig.8cASC.tif
- Fig.8cNLRP3.tif
- Fig.8ccaspase1.tif
- Fig.8cactin.tif
- Fig1.cLCN2.tif
- Fig1.cactin.tif
- Fig1.eLCN2.tif
- Fig1.eactin.tif
- FigureS1.tif
- FigureS2.tif
- FigureS3.tif